Acceleration Measurement Using the Laser Doppler Technique

by

B. Lehmann[†], H. Nobach[‡] and C. Tropea[‡]

[†] Deutsches Zentrum für Luft- und Raumfahrt, Institut für Antriebstechnik, Abteilung Turbulenzforschung, Müller-Breslau-Straße 8, 10623 Berlin, Germany

[‡] Fachgebiet Strömungslehre und Aerodynamik, Petersenstraße 30, 64287 Darmstadt, Germany

ABSTRACT

Generally, the laser Doppler and phase Doppler techniques are considered point measurement techniques, because they achieve a high enough spatial resolution that the measured quantities can be considered constant over the transit time of the tracer particle or dispersed particle through the measurement volume. In most applications this is an appropriate assumption and the signal processing must provide only one single value of each velocity component or particle size for each particle. However, in some situations this may not be sufficient.

The phase difference in a phase Doppler system can vary when an oscillating droplet passes through the measurement volume. Appropriate signal processing can provide considerable information about droplet shape and oscillation frequency/state by estimating these phase difference variations within one signal. Similarly, a tracer particle or dispersed particle under acceleration results in a change of Doppler signal frequency during passage through the detection volume of a laser Doppler system (figure 1). This information can be interpreted directly as the material derivative of the particle velocity, and is an important quantity in the formulation of Lagrangian stochastic models for simulating turbulent flows in which transport is of primary interest.

However, existing signal processors for the laser Doppler technique do not attempt estimates of this frequency variation, despite the fact of that most processors are now fully digitally based and could implement — possibly in firmware — virtually any parameter estimator. Acceleration can be measured using a laser Doppler system by estimating the change of signal frequency with time. Three estimators are introduced for estimating the acceleration parameter from Doppler signals (figure 2). The performance is evaluated by examining the bias and comparing the variance to the Cramér-Rao Lower Bound. Validation experiments are performed in a laminar stagnation flow.

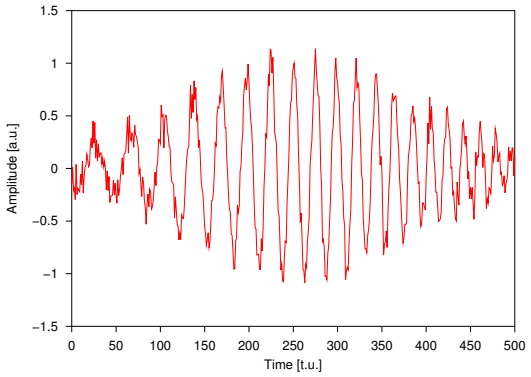

Figure 1: A simulated burst signal of an accelerated particle with added noise

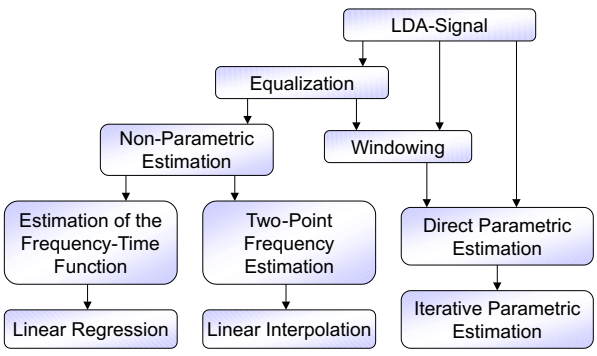

Figure 2: Classification of the signal processing algorithms

1. INTRODUCTION

Measuring the acceleration of a tracer particle in a flow provides a direct estimate of the Lagrangian material derivative, e.g. for a cartesian coordinate system and for the u velocity component

$$\underbrace{\frac{\mathrm{D}u}{\mathrm{D}t}}_{\substack{\text{Lagrangian}\\ \text{acceleration}\\ \text{(material}\\ \text{derivative)}}} = \underbrace{\underbrace{\frac{\partial u}{\partial t}}_{\substack{\text{temporal}\\ \text{acceleration}}} + \underbrace{u\frac{\partial u}{\partial x} + v\frac{\partial u}{\partial y} + w\frac{\partial u}{\partial z}}_{\substack{\text{advective}\\ \text{acceleration}}}}_{\text{Eulerian acceleration}} \tag{1}$$

In principal therefore, the laser Doppler technique, particle tracking velocimetry (PTV) or particle image velocimetry (PIV) can be used to estimate the Lagrangian acceleration if temporal changes of velocity can be registered. Christensen and Adrian [3] have recently explored this possibility with PIV, presenting as a first step an estimation of the possible accuracy in the presence of noise.

There are various motivations for measuring the Lagrangian acceleration in turbulent flows. These all relate to the fact that the Lagrangian acceleration appears on the left-hand-side of the Navier-Stokes equations, e.g. in cartesian coordinates omitting body forces and for an incompressible, Newtonian fluid

$$\frac{\mathrm{D}u_i}{\mathrm{D}t} = \frac{\partial u_i}{\partial t} + u_j\frac{\partial u_i}{\partial x_j} = -\frac{1}{\varrho}\frac{\partial p}{\partial x_i} + \nu\frac{\partial^2 u_i}{\partial x_j \partial x_j} \tag{2}$$

where ν is the kinematic viscosity of the fluid. Thus, the fluid particle acceleration can be attributed to pressure gradient and viscous forces. Hill and Thoroddsen [7] attempted to measure the fluid-particle acceleration by measuring the right-hand-side of equation (2) using hot-wire anemometry, Taylor's hypothesis and assuming local isotropy. They conclude that a spatial resolution on the order of the Kolmogorov microscale is needed to obtain the acceleration due to the viscous force, whereas about half that resolution is needed for the pressure-gradient correlation. A direct measurement of the Lagrangian correlation would therefore be very attractive if then such spatial resolution requirements could be relaxed.

Lagrangian stochastic models using fluid-particle acceleration have been proposed for simulating turbulent flows in which transport is of primary interest. Such statistics were already discussed in Lin [15] or in Monin and Yaglom [18] for isotropic, homogeneous turbulence. Most models refer back to Kolmogorov's 1941 hypotheses [10, 11], which to date have not been tested.

Acceleration is often discussed in relation to Taylor's hypothesis, which essentially postulates that the local and advective terms of acceleration cancel [6], i.e. for a one-dimensional flow $\partial/\partial t = u\partial/\partial x$. Most studies to date examine acceleration using direct numerical simulations and are restricted therefore to relatively low Reynolds numbers [23, 25, 28]. Experimental investigations of fluid acceleration statistics are not abundant but do include studies using various techniques: hot-wire anemometry [7], particle tracking [27] and most recently particle-imaging velocimetry [3].

For locally isotropic turbulence, the mean square of the turbulent acceleration can be expressed as

$$\langle a_i a_j \rangle = a_0 \varepsilon^{3/2} \nu^{-1/2} \delta_{ij} \tag{3}$$

where ε is the rate of dissipation of mechanical energy per unit mass and a_0 is a universal numerical constant ([18], p.369). Hence, a measurement of local acceleration does provide a means for estimating dissipation rate in some cases. Since $\varepsilon \propto U^3/L$ [26], where U and L are characteristic velocity and length scales then

$$\langle a_i a_i \rangle^{1/2} \propto U^{9/4} / \left(L^{3/4} \nu^{1/4} \right) \tag{4}$$

This indicates that the turbulent acceleration fluctuations will increase rapidly with an increasing characteristic velocity U.

More recently, Voth *et al* [27] have questioned over what Reynolds number range a_0 can still be considered constant. A direct measurement of acceleration in a flow with known dissipation dependencies, e.g. a turbulent free jet, would allow this hypothesis to be tested directly [19].

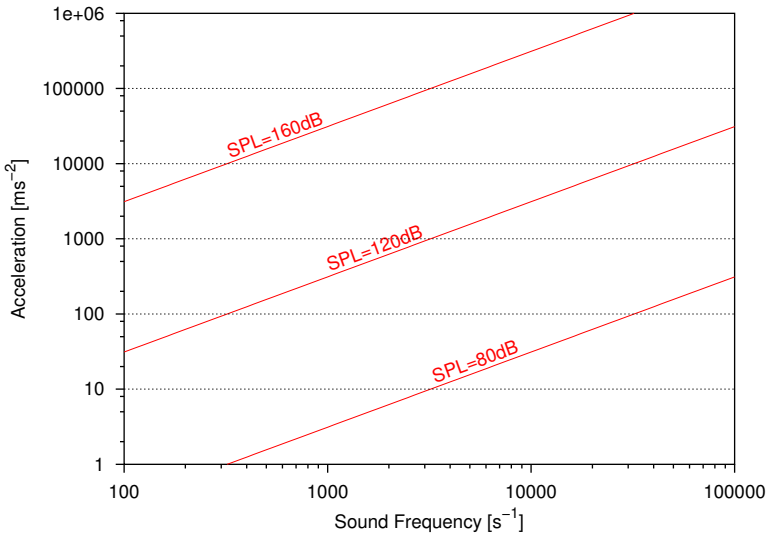

Figure 3: Relation between the sound frequency and the acceleration

A second motivation for measuring acceleration can be found in the field of acoustics, namely to measure directly the local sound pressure level (SPL) in dB. Figure 3 reflects the relation between the frequency and the acceleration for typical values of the medium density ($1.18\,\mathrm{kg/m^3}$) the sound speed ($340\,\mathrm{m/s}$) and the SPL.
In the following section several estimators of signal frequency changes are introduced. This is followed by an evaluation of their performance using simulated signals (section 3). In section 4 an experiment is presented to validate the estimators. Also the important question of tracer-particle slip is addressed. Finally, in section 5 some overall conclusions are drawn.

2. ESTIMATION OF SIGNAL FREQUENCY VARIATIONS

In this section three estimators for the changes of frequency within a single laser Doppler signal are introduced and their performance is studied using simulated signals. All estimators investigated use a signal model as a basis and these models are first introduced, together with the pre-processing steps required to meet the constraints of the respective models. The three estimators can be classified as non-parametric, direct parametric and iterative parametric (figure 4), in increasing degree of complexity. The estimators have several options of signal processing details (windowing, weighting, spectral interpolation) as indicated in figure 4, leading to a non-usable number of different algorithms. However, these options are discussed more generally, since the influence to the estimation results are similar for these three estimator classes.

2.1 Signal Model and Pre-processing Steps

Particle acceleration is detected in the laser Doppler technique by a change of signal frequency. The simplest signal model incorporating such acceleration is therefore a sine wave with a linear change in time of the fundamental frequency

$$f(t) = \gamma(t - T) + f_\mathrm{m} \tag{5}$$

where γ is the acceleration coefficient [t.u.$^{-2}$] (t.u.=arbitrary time unit) and f_m [t.u.$^{-1}$] is the signal frequency at the midpoint of the burst $t = T$, known also as the arrival time or time of maximum signal amplitude. The particle acceleration a [m/t.u.^{2}] is obtained using $a = \gamma\Delta x$, where Δx is the interference fringe spacing of the laser Doppler system. The use of an arbitrary time unit instead of dimensional time units indicates that the estimation procedures can be scaled arbitrarily. Therefore, it is possible to use the algorithms and results for very fast and also for slow processes without changes.

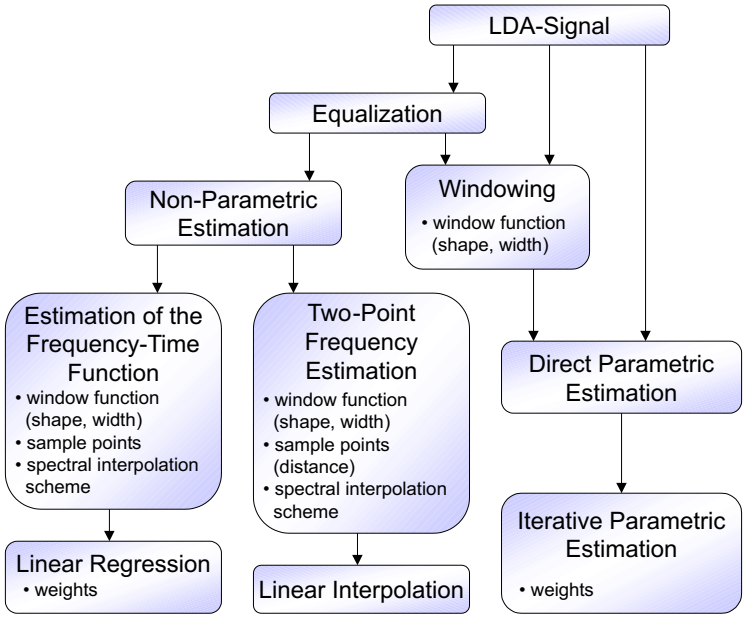

Figure 4: Classification of the signal processing algorithms with specific options

Using equation (5) for the instantaneous frequency a corresponding signal model can be derived. The change of signal phase with time is simply

$$\frac{\partial \varphi}{\partial t} = 2\pi f(t) = 2\pi \left[\gamma(t-T) + f_\mathrm{m}\right], \tag{6}$$

and integration yields the instantaneous phase

$$\varphi(t) = \pi\gamma(t-T)^2 + 2\pi f_\mathrm{m}(t-T) + \phi \tag{7}$$

An approprate signal then becomes

$$u(t) = A(t-T)\cos\left[\pi\gamma(t-T)^2 + 2\pi f_\mathrm{m}(t-T) + \phi\right] \tag{8}$$

where $A(t-T)$ is the envelope amplitude. Using a discrete signal with a Gaussian envelope yields

$$u(t_k) = A\exp\left[-\eta(t_k-T)^2\right]\cos\left[\pi\gamma(t_k-T)^2 + 2\pi f_\mathrm{m}(t_k-T) + \phi\right] \quad k = 0\ldots N-1 \tag{9}$$

with the burst width parameter η [t.u.$^{-2}$]. Figure 5 illustrates a simulated burst signal from an accelerated particle, including added white noise.
By estimating the instantaneous Doppler frequency $\hat{f}(t)$ throughout the burst, the midpoint frequency f_m and the acceleration parameter γ can be derived directly using a linear fit to the data. However, any estimate of the instantaneous Doppler frequency requires a finite number of data samples from the signal. Therefore, to obtain the Doppler frequency as a function of the time, a sliding window is required, in the most simple case a rectangular function. However, this window function is not well suited to Doppler bursts, since the signal amplitude at the window edges is high, hence the window truncates the signal. This leads to a biased frequency estimate. Therefore, smooth window functions are preferred, e.g. Hanning, Hamming or Blackman windows.
A second effect leading to biased frequency estimates is the influence of the signal amplitude as a weighting factor. The varying amplitude at the tails of the burst signal leads to an asymmetry in the time domain, hence to a distorted spectrum with a translation of the maximum peak. A frequency estimation based on a spectral peak interpolation does not lead to an accurate estimate of the midpoint frequency f_m. Therefore, an equalization of the signal amplitude throughout the burst is required. This can be achieved by using a normalization with the instantaneous amplitude of the envelope. The envelope of the burst

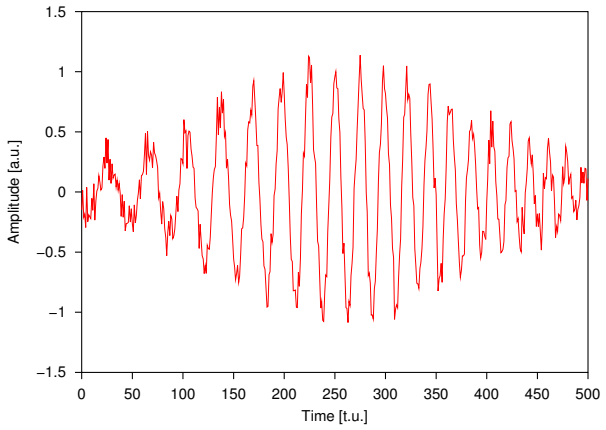

Figure 5: A simulated burst signal from an accelerated particle with added noise.

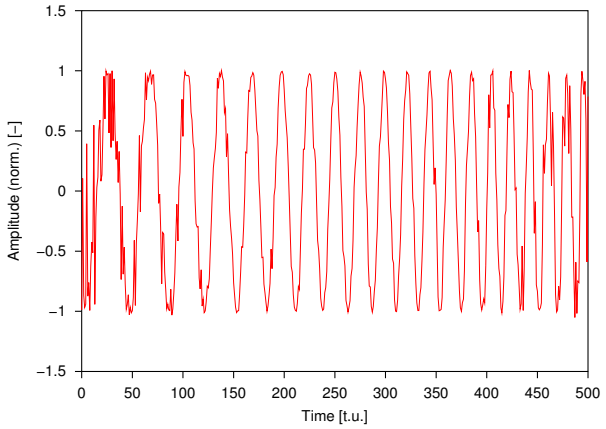

Figure 6: Amplitude-equalized Doppler burst from an accelerated particle.

signal can be calculated from the analytical signal, which can be derived using the Hilbert transform $\mathcal{H}$ [1]. The equalized signal $\tilde{u}(t_k)$ then can be calculated through

$$\tilde{u}(t_k) = \frac{\hat{u}(t_k)}{|\hat{u}(t_k) + i\mathcal{H}\{\hat{u}\}(t_k)|} \tag{10}$$

with the imaginary unit i and the (noisy) measured signal $\hat{u}(t_k)$. Figure 6 shows the result of the equalization using the simulated burst from figure 5.
Note, that the equalization procedure removes all information related to the envelope of the signal, including the arrival time and the burst width. Therefore, the signal detection and acquisition must be performed very carefully to insure that the signal is centered within the observation window, thus avoiding biased midpoint frequency estimates. Furthermore, the burst width and arrival time estimates are not related to the signal anymore. They are given through the window function, which influences the derivation of the CRLB.

2.2 Non-Parametric Estimation

A sliding window is passed over the equalized burst signal; in this case a Hanning window with a width of 150 t.u. is used. For each point in time, the instantaneous Doppler frequency is estimated using the spectral peak interpolation method based on a parabolic fit to the maximum point in the logarithmic spectrum and the two neighbouring points [5, 8]. Since the frequency is a statistical value, these are only averaged estimates over the window width. Therefore, the estimated frequency-time function has only

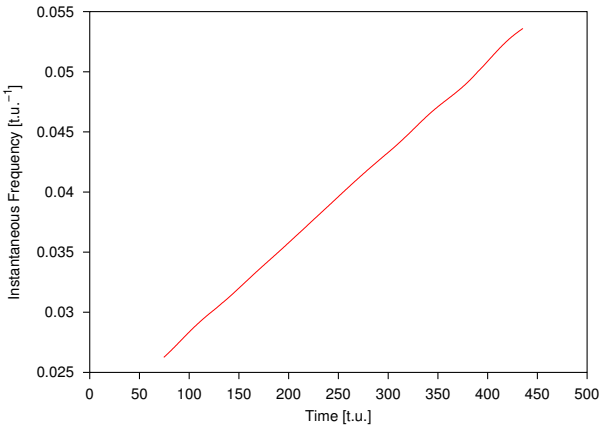

Figure 7: The frequency-time function of the Doppler burst from an accelerated particle.

a limited dynamic response. However, this is important only for non-linear frequency changes, while a linear dependence can be correctly captured (figure 7).
A linear fit to the frequency-time function yields directly the midpoint frequency f_m and the frequency gradient γ. However, the calculation of the complete frequency-time function is costly. A useful simplification of the procedure is to calculate the instantaneous frequency at only two points T_1 and $T_2 = T_1 + \Delta T$ and to derive the frequency parameters directly as

$$f_\mathrm{m} = \frac{\hat{f}(T_1) + \hat{f}(T_2)}{2} \tag{11}$$

$$\gamma = \frac{\hat{f}(T_2) - \hat{f}(T_1)}{\Delta T} \tag{12}$$

This is the estimation procedure described in [12, 13], which is found to be very robust. Note that these authors used a linear spectral interpolation scheme [16].
The window type, width and the location of the two windows relative to the burst center are parameters of the method, which can optimize the estimation results in terms of bias and estimation variance. In this study the entire signal is split at the midpoint and the two windows (Hanning) are centered over the two subsignals.

2.3 Direct Parametric Estimation

For an assumed signal of the form given in equation (9), a direct parameter estimator in the frequency domain is now introduced. To derive the Fourier transform of this signal, first the reduced model without acceleration

$$u(t_k) = A \exp\left[-\eta(t_k - T)^2\right] \cos\left[2\pi f_\mathrm{D}(t_k - T) + \phi\right] \quad k = 0 \ldots N-1 \tag{13}$$

is discussed. Using

$$\cos x = \frac{e^{ix} + e^{-ix}}{2} \tag{14}$$

with the imaginary unit i, the following expression for the signal is obtained.

$$\begin{aligned} u(t_k) = &\frac{A}{2} \exp\left\{-\eta(t_k - T)^2 + i\left[2\pi f_\mathrm{D}(t_k - T) + \phi\right]\right\} \\ &+ \frac{A}{2} \exp\left\{-\eta(t_k - T)^2 - i\left[2\pi f_\mathrm{D}(t_k - T) + \phi\right]\right\}. \end{aligned} \tag{15}$$

The discrete Fourier transform of this signal is

$$\mathcal{D}\{u(t_k)\}(f_j) = \sum_{k=0}^{N-1} u(t_k)\exp(-2\pi \mathrm{i} f_j t_k) = \sum_{k=0}^{N-1} u(t_k)\exp(-2\pi \mathrm{i} kj/N) \tag{16}$$

$$\begin{aligned} &= \frac{Af_\mathrm{s}}{2}\left(\frac{\pi}{\eta}\right)^{\frac{1}{2}} \exp\left[-\pi^2(f_j - f_\mathrm{D})^2\eta^{-1} - \mathrm{i}(2\pi f_j T - \phi)\right] \\ &\quad + \frac{Af_\mathrm{s}}{2}\left(\frac{\pi}{\eta}\right)^{\frac{1}{2}} \exp\left[-\pi^2(f_j + f_\mathrm{D})^2\eta^{-1} - \mathrm{i}(2\pi f_j T + \phi)\right] \end{aligned} \tag{17}$$

where $f_\mathrm{s} = 1\,\mathrm{t.u.}^{-1}$ is the sampling frequency.
For the signal model with acceleration, the term $\pi\gamma(t_k - T)^2$ appears and η can be replaced by $\eta - \mathrm{i}\pi\gamma$ or $\eta + \mathrm{i}\pi\gamma$ respectively, which leads to

$$\begin{aligned} u(t_k) &= \frac{A}{2}\exp\left\{-\eta(t_k - T)^2 + \mathrm{i}\left[\pi\gamma(t_k - T)^2 + 2\pi f_\mathrm{m}(t_k - T) + \phi\right]\right\} \\ &\quad + \frac{A}{2}\exp\left\{-\eta(t_k - T)^2 - \mathrm{i}\left[\pi\gamma(t_k - T)^2 + 2\pi f_\mathrm{m}(t_k - T) + \phi\right]\right\} \\ &= \frac{A}{2}\exp\left\{-(\eta - \mathrm{i}\pi\gamma)(t_k - T)^2 + \mathrm{i}\left[2\pi f_\mathrm{m}(t_k - T) + \phi\right]\right\} \\ &\quad + \frac{A}{2}\exp\left\{-(\eta + \mathrm{i}\pi\gamma)(t_k - T)^2 - \mathrm{i}\left[2\pi f_\mathrm{m}(t_k - T) + \phi\right]\right\} \end{aligned} \tag{18}$$

and for the discrete Fourier transform

$$\begin{aligned} \mathcal{D}\{u(t_k)\}(f_j) &= \frac{Af_\mathrm{s}}{2}\left(\frac{\pi}{\eta - \mathrm{i}\pi\gamma}\right)^{\frac{1}{2}} \exp\left[-\pi^2(f_j - f_\mathrm{m})^2(\eta - \mathrm{i}\pi\gamma)^{-1} - \mathrm{i}(2\pi f_j T - \phi)\right] \\ &\quad + \frac{Af_\mathrm{s}}{2}\left(\frac{\pi}{\eta + \mathrm{i}\pi\gamma}\right)^{\frac{1}{2}} \exp\left[-\pi^2(f_j + f_\mathrm{m})^2(\eta + \mathrm{i}\pi\gamma)^{-1} - \mathrm{i}(2\pi f_j T + \phi)\right] \end{aligned} \tag{19}$$

Assuming no interference of the spectral peaks at f_m and $-f_\mathrm{m}$ and all repetitions thereof, only the range of frequencies between 0 and $f_\mathrm{s}/2$ is required, yielding

$$\mathcal{D}\{u(t_k)\}(f_j) = \frac{Af_\mathrm{s}}{2}\left(\frac{\pi}{\eta - \mathrm{i}\pi\gamma}\right)^{\frac{1}{2}} \exp\left[-\pi^2(f_j - f_\mathrm{m})^2(\eta - \mathrm{i}\pi\gamma)^{-1} - \mathrm{i}(2\pi f_j T - \phi)\right] \tag{20}$$

Using the substitution

$$\eta - \mathrm{i}\pi\gamma = B\mathrm{e}^{\mathrm{i}P} = \exp(\ln B + \mathrm{i}P) \tag{21}$$

the discrete Fourier transform becomes

$$\begin{aligned} \mathcal{D}\{u(t_k)\}(f_j) = \frac{Af_\mathrm{s}\sqrt{\pi}}{2}\exp\Bigg[&-\frac{\ln B}{2} - \mathrm{i}\frac{P}{2} - \pi^2(f_j - f_\mathrm{m})^2 \\ &\times \exp(-\ln B - \mathrm{i}P) - \mathrm{i}(2\pi f_j T - \phi)\Bigg] \end{aligned} \tag{22}$$

and its complex logarithm

$$\begin{aligned} \ln\{\mathcal{D}\{u(t_k)\}(f_j)\} = \ln\left(\frac{Af_\mathrm{s}\sqrt{\pi}}{2}\right) - \frac{\ln B}{2} - \frac{\pi^2\cos(-P)}{B}(f_j - f_\mathrm{m})^2 \\ + \mathrm{i}\left[-2\pi f_j T + \phi - \frac{P}{2} - \frac{\pi^2\sin(-P)}{B}(f_j - f_\mathrm{m})^2\right] \end{aligned} \tag{23}$$

yields the amplitude and the phase spectrum, which both are of second order.

$$\ln\{\mathcal{D}\{u(t_k)\}(f_j)\} = \underbrace{a_1(f_j - f_\mathrm{m})^2 + c_1}_{\text{amplitude spectrum}} + \mathrm{i}\underbrace{[a_2(f_j - f_\mathrm{m})^2 + b_2(f_j - f_\mathrm{m}) + c_2]}_{\text{phase spectrum}} \tag{24}$$

with

$$a_1 = -\frac{\pi^2 \cos(-P)}{B} \tag{25}$$

$$c_1 = \ln\left(\frac{A\sqrt{\pi}}{2}\right) - \frac{\ln B}{2} \tag{26}$$

$$a_2 = -\frac{\pi^2 \sin(-P)}{B} \tag{27}$$

$$b_2 = -2\pi T \tag{28}$$

$$c_2 = \phi - \frac{P}{2} - 2\pi f_\mathrm{m} T. \tag{29}$$

With the argument $f_j - f_\mathrm{m}$, the parabola of the amplitude spectrum has no linear part. Hence, the Doppler frequency can be derived from the maximum of the amplitude spectrum even with an acceleration. This is the reason why a normal spectral interpolation technique can be used to estimate the center frequency of a burst from an accelerated particle. Since this is also valid for a part of the burst, the non-parametric method described above is able to derive the correct center frequency for each window position.
This analysis leads directly to an appropriate estimation procedure. The measured discrete burst signal $\hat{u}(t_k)$ is transformed to the frequency domain

$$\hat{U}(f_j) = \mathcal{D}\{\hat{u}(t_k)\} \tag{30}$$

using the discrete Fourier transform (equation (16)). The absolute magnitude and the argument of this complex function yield the amplitude spectrum $|\hat{U}(f_j)|$ and the phase spectrum $\hat{\varphi}(f_j) = \arg(\hat{U}(f_j))$. In the amplitude spectrum $|\hat{U}(f_j)|$, the maximum is sought. The logarithm of the maximum value and the two neighbours is the base for a three-point parabolic interpolation of the frequency. The midpoint frequency $\hat{f}_\mathrm{m}$ corresponds to the frequency at which the maximum point of the parabola occurs. This procedure is similar to the spectral peak interpolation for the case without acceleration, except that now the absolute magnitude of the discrete Fourier transform is used directly instead of the power spectral density.
After the correction of 2π ambiguities, a parabolic interpolation is also performed in the phase spectrum. The coefficients of both interpolation parabolas (logarithmic amplitude and phase spectrum) have to be transformed to the argument $f - \hat{f}_\mathrm{m}$. Hence the linear coefficient of the parabola in the logarithmic amplitude spectrum disappears. The other coefficients are as in equation (24). For these coefficients the system of equations (25)–(29) leads to

$$B = \frac{\pi^2}{|a_1 + \mathrm{i}a_2|} \tag{31}$$

$$P = \arg\{-a_1 + \mathrm{i}a_2\} \tag{32}$$

$$\hat{\gamma} = -\frac{B}{\pi}\sin P \tag{33}$$

$$\hat{\eta} = B\cos P \tag{34}$$

$$\hat{T} = -\frac{b_2}{2\pi} \tag{35}$$

$$\hat{A} = \frac{2}{f_\mathrm{s}\sqrt{\pi}} \exp\left(c_1 + \frac{\ln B}{2}\right) \tag{36}$$

$$\hat{\phi} = c_2 + \frac{P}{2} + 2\pi f_\mathrm{m} T \tag{37}$$

This procedure yields reliable results for signals resembling the assumed model. However, it is very sensitive to distortions of the envelope. The effect is significant, since the model does not consider the correlation of the burst length and the particle velocity. This leads to a distorted envelope for accelerated particles because of the varying velocity during the passage of the measurement volume. Furthermore, the

signal envelope is influenced by slits on the receiving aperture, non-linear amplifiers, filters and window functions. Thus, the direct estimator generally yields biased results.
To improve this estimate, an equalization of the signal amplitude using equation (10) and a windowing function are performed. Because of the sensitivity of the procedure to distortions of the envelope only a Gaussian window is appropriate.

$$w(t_k) = \exp\left[-\xi\left(\frac{k}{N-1} - \frac{1}{2}\right)^2\right] \tag{38}$$

The signal $u(t_k)$ is presumed to be centered in the signal record with $T_\mathrm{m} = (N-1)/(2f_\mathrm{s})$. The width parameter ξ can be chosen arbitrarily, an acceptable compromise between the estimation bias and the estimation variance can be obtained using $\xi = 40$.

2.4 Iterative Parametric Estimator

The aim of an iterative parameter estimator is to improve (optimize) a parameter set stepwise, leading to a model of the signal $u(t_k)$ which is as close as possible to the measured signal $\hat{u}(t_k)$. As a figure of merit, the L_2 norm

$$e = \sum_{k=0}^{N-1} w_k \left[\hat{u}(t_k) - u(t_k)\right]^2 \tag{39}$$

is normally used, which has to be minimized (method of least squares). For Gaussian distributed noise, this leads to the maximum likelihood estimator. For other noise distributions, this is not the best estimator. However, in most cases the accuracy of the L_2 norm is sufficient and the estimation is very robust. The additional weighting factors w_k are necessary in the case of non-constant noise power. They can be used to suppress the influence of very noisy signal parts to the results and to emphasize signal parts with low noise.
Ideally, the minimum of the L_2 norm could be derived explicitly; however, this is only possible for very simple signal models. Normally therefore, the minimization of the L_2 norm proceeds iteratively, improving the model parameters stepwise. The initial parameter set can be obtained using for example one of the procedures described before.
Since the signal is influenced by various effects which distort the envelope, the ideal burst model (equation (9)) is not practicable for real signals. To obtain signals with a known envelope a pre-processing step is necessary, e.g. the equalization step of the non-parametric estimator (equation (10)), yielding the signal $\tilde{u}(t_k)$ with a constant amplitude of 1. The appropriate signal model is then

$$u(t_k) = \cos\left[\pi\gamma(t_k - T)^2 + 2\pi f_\mathrm{m}(t_k - T) + \phi\right] \tag{40}$$

with the parameter vector

$$\alpha = \begin{bmatrix} \gamma \\ f_\mathrm{m} \\ \phi \end{bmatrix} \tag{41}$$

Since the equalization yields a signal with time dependent noise power, a Hanning window

$$w_k = 0.5 - 0.5\cos\left(\frac{2\pi k}{N-1}\right) \tag{42}$$

is used as a weighting function. The original signal is presumed to be centered in the signal record with $T_\mathrm{m} = (N-1)/(2f_\mathrm{s})$.
The parameter optimum is then given through the system of equations

$$\begin{pmatrix} \frac{\partial e}{\partial \gamma} \\ \frac{\partial e}{\partial f_\mathrm{m}} \\ \frac{\partial e}{\partial \phi} \end{pmatrix} = 0 \tag{43}$$

Table 1: Parameter specification for the bias investigation

Parameter	value	unit	specification
N	512	–	
T	255.5	t.u.	$0.5(N-1)$ t.u.
η	3.06×10^{-5}	t.u.$^{-2}$	$8(N-1)^{-2}$ t.u.$^{-2}$
A	1.0	a.u.	
γ	$1.0 \times 10^{-6} \ldots 1.5 \times 10^{-4}$	t.u.$^{-2}$	
f_m	0.04	t.u.$^{-1}$	
ϕ	$0 \ldots 2\pi$	rad	

To solve this system, a tangent algorithm is used, leading to the iteration step from the (n)-th to the $(n+1)$-st estimate

$$\begin{pmatrix} \frac{\partial^2 e}{\partial \gamma^2} & \frac{\partial^2 e}{\partial \gamma \partial f_\mathrm{m}} & \frac{\partial^2 e}{\partial \gamma \partial \phi} \\ \frac{\partial^2 e}{\partial \gamma \partial f_\mathrm{m}} & \frac{\partial^2 e}{\partial f_\mathrm{m}^2} & \frac{\partial^2 e}{\partial f_\mathrm{m} \partial \phi} \\ \frac{\partial^2 e}{\partial \gamma \partial \phi} & \frac{\partial^2 e}{\partial f_\mathrm{m} \partial \phi} & \frac{\partial^2 e}{\partial \phi^2} \end{pmatrix} \begin{pmatrix} \gamma^{(n)} - \gamma^{(n+1)} \\ f_\mathrm{m}^{(n)} - f_\mathrm{m}^{(n+1)} \\ \phi^{(n)} - \phi^{(n+1)} \end{pmatrix} + \begin{pmatrix} \frac{\partial e}{\partial \gamma} \\ \frac{\partial e}{\partial f_\mathrm{m}} \\ \frac{\partial e}{\partial \phi} \end{pmatrix} = 0 \tag{44}$$

To prevent divergence after each iteration step, the parameter range and the convexity of the figure-of-merit are monitored using

$$0 < f_\mathrm{m} < f_\mathrm{s}/2 \tag{45}$$

$$\frac{\partial^2 e}{\partial \gamma^2} > 0 \tag{46}$$

$$\frac{\partial^2 e}{\partial f_\mathrm{m}^2} > 0 \tag{47}$$

Note that the convexity check is not necessary for the phase, because of its periodicity.
This procedure yields bias free and almost efficient estimates of the midpoint frequency f_m and the acceleration parameter γ over a wide range of signal parameters. However, this iterative procedure requires reliable pre-estimates of the parameters. Therefore, the maximum allowable noise power is dictated by the pre-estimation procedure used. The non-parametric estimation also yields reliable results with a fraction of the computational costs. On the other hand, the possibility to expand the signal model to higher order derivatives of the velocity may be an important advantage for some applications.

3. NUMERICAL SIMULATIONS

To demonstrate the performance of the estimation routines, a numerical simulation has been performed using the signal

$$\hat{u}(t_k) = A \exp\left[-\eta (t_k - T)^2\right] \cos\left[\pi \gamma (t_k - T)^2 + 2\pi f_\mathrm{m} (t_k - T) + \phi\right] \quad k = 0 \ldots N-1 \tag{48}$$

which is equal to the signal model (equation (9)). The signal parameters are given in table 1. To obtain the influence of the acceleration parameter, the true γ was varied in 25 steps between 0.00001 t.u.$^{-2}$ and 0.0003 t.u.$^{-2}$.
For each simulated and equalized signal, the acceleration parameter γ were calculated using the three estimators with a Hanning window/weighting scheme and with a Gauss window/weighting scheme.
In figure 8a the empirical expectation of the three estimation methods are shown for a Hanning window/weighting scheme. The direct parametric method clearly shows a varying bias over the varied acceleration parameter γ. The bias of the other two methods is significantly smaller. The cause of the biased estimates of the direct parametric method is the non-ideal window function. This method uses the parabola interpolation to estimate the parameters. As shown in the derivation of the method, this is suitable only for a Gaussian envelope of the signal. A function with an envelope obtained by a Hanning window leads to biased estimates of the acceleration parameter.

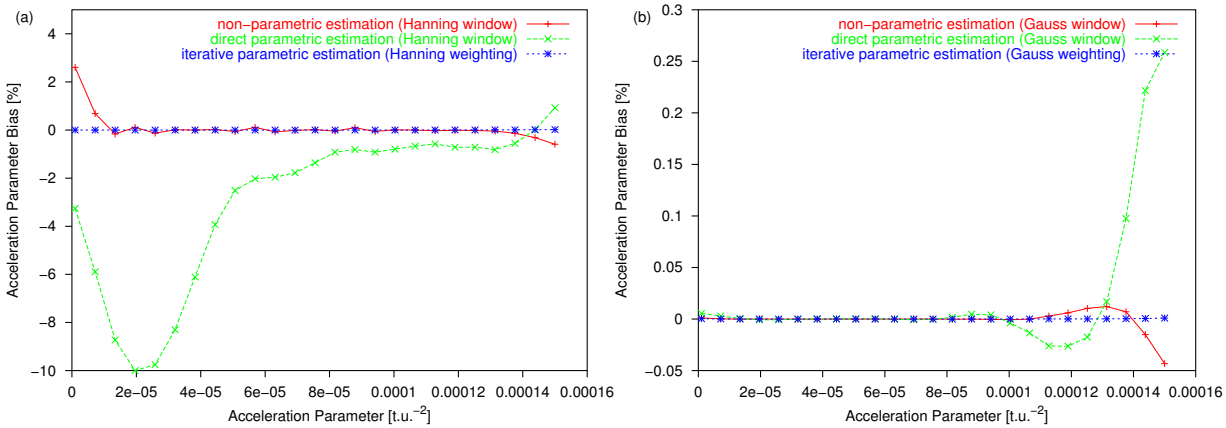

Figure 8: Bias of the acceleration parameter estimate (a) Hanning window/weighting and (b) Gauss window/weighting.

Table 2: Parameter specification for the estimation variance investigation

Parameter	value	unit	specification
N	512	–	
T	255.5	t.u.	$0.5(N-1)$ t.u.
η	3.06×10^{-5}	t.u.$^{-2}$	$8(N-1)^{-2}$ t.u.$^{-2}$
A	1.0	a.u.	
γ	7.5×10^{-5}	t.u.$^{-2}$	
f_m	0.04	t.u.$^{-1}$	
ϕ	$0 \ldots 2\pi$	rad	
σ_n^2	0.01	a.u.^{2}	

Better results can be obtained using the Gauss window, which can improve also the performance of the non-parametric method. An appropriate weighting scheme can be applied to the iterative parameter estimation. Figure 8b shows the results of the modified methods. The bias of both, the direct parametric and the non-parametric method, is reduced significantly.
In both diagramms the iterative paramtric estimation is clearly superior. It has almost no bias over the entire range of the acceleration parameter variation. Furthermore, this is independent of the used weighting scheme (Hanning or Gauss), indicating the high robustness of this estimator.
A second numerical simulation was performed to derive the estimation variance of the methods using the signal

$$\begin{aligned}\hat{u}(t_k) = A \exp\left[-\eta(t_k - T)^2\right] \\ \times \cos\left[\pi\gamma(t_k - T)^2 + 2\pi f_\mathrm{m}(t_k - T) + \phi\right] + n_k \qquad k = 0 \ldots N-1\end{aligned} \tag{49}$$

which is the same signal model as used above but with an additional noise component n_k. The signal parameters are given in table 2. The noise is uncorrelated and Gaussian distributed. 1 000 independent realisations were generated to derive the empirical variance of the estimation.
Table 3 shows the efficiency of the estimation methods as a ratio of the Cramér-Rao Lower Bound (CRLB) [9, 20, 22] to the empirical estimation variance of the acceleration parameter. The higher this ratio the better the algorithm. A value of 1.0 indicates an efficient estimator.
No algorithm reaches the CRLB, because all require the equalization step to derive an envelope-independent signal. This reduces the information content of the signal. The iterative parameter estimation comes closest to the CRLB compared to the other statistical methods. In all cases the modified algorithms using a Gauss window/weighting scheme have a higher estimation variance than the original procedures using the Hanning window/weighting scheme. The Gaussian window/weighting function can be scaled in

Table 3: Efficiency of the estimation methods (estimation of the acceleration parameter) given as the CRLB-to-estimation variance ratio

Estimation Method	Hanning Window/Weighting	Gauss Window/Weighting
Non-Parameric	0.182	0.134
Direct Parameric	0.002	0.020
Iterative Parameric	0.723	0.262

width. However, this is always a compromise between the bias due to the non-zero values at the edges of the window and the usable signal information. To insure a very low estimation bias, the window must be chosen narrow. On the other hand, this reduces the usable signal information and increases the estimation variance, which is the price paid for the smaller bias. The direct parametric estimation, however, is very sensitive to deviations of the envelope shape and yields reliable results only for the narrow Gaussian window function.
In summary, of the three investigated estimators for the acceleration, the iterative parametric estimator consistently yields the lowest bias and variance. The direct parametric estimate can be significantly improved using a Gauss amplitude window. The bias of the non-parametric estimate can also be reduced using a Gauss amplitude window. However, the estimation variance increases. This is the price paid for the smaller bias. On the other hand, this method exhibits a lower sensitivity to envelope irregularities than the other estimators, i.e. it is quite robust and, compared to the iterative parametric estimation, it is very simple.

4. EXPERIMENTAL INVESTIGATIONS

To illustrate the measurement of particle acceleration, a steady stagnation flow has been used. A one-velocity component laser Doppler system working with a He-Ne laser (15 mW) in forward scatter was used. The full intersection angle was 7.7°. The e^{-1} diameter of the illumination volume was 330 µm and the maximum number of stationary fringes was 70 (4.7 µm fringe spacing). A beam waist adjustment was used in the transmitting optics to position the beam waist at the point of beam intersection. With a Rayleigh length of approximately 100 mm, the fringe non-uniformities according to Miles [17] will be insignificant within the measurement accuracy of this system. A set frequency shift of 3.281 MHz (±0.2 %) was applied using a rotating grating. A filter of bandwidth 1 MHz to 12 MHz was used prior to digitisation. The signal frequency was in the range 3 MHz to 6 MHz, thus no significant influence of the filters on the spectral content of the signal was expected. Atomized droplets with a maximum diameter of 2 µm were used as tracer particles generated by a Dantec SAFEX fog generator (30 % indide fog fluid/standard and 70 % water).
The signals were digitized using a transient recorder (70 Msamples/s, 512 samples) and processed using the non-parameteric estimator (Hanning window). The maximum measurable mean velocity, accounting for acceleration, was about 15 m/s. At each measurement point 4 000 signals were used to compute mean statistics.
The stagnation flow consisted of a free air jet issuing from a 35 mm diameter nozzle into a 200 mm diameter and 300 mm long chamber with diametrically opposed windows. A cylindrical rod of diameter $d = 5$ mm was positioned on the jet axis such that its flat end face was 1.5 nozzle diameters from the nozzle exit. Measurements of the axial velocity component were performed along the jet centerline. The results of these measurements are shown in figure 9, using as an abscissa the normalized distance from the stagnation surface, x/d.
Figure 9a shows the mean velocity, normalized with the centerline velocity far removed from the stagnation surface. Figure 9b shows the local turbulence level, i.e. the measured standard deviation of the velocity fluctuations divided by the local mean velocity. These results indicate that the flow is laminar, with an asymptotic turbulence level far from the cylinder of less than 2 %.
For this steady flow and for measurements along the jet centerline the material derivative of the particle

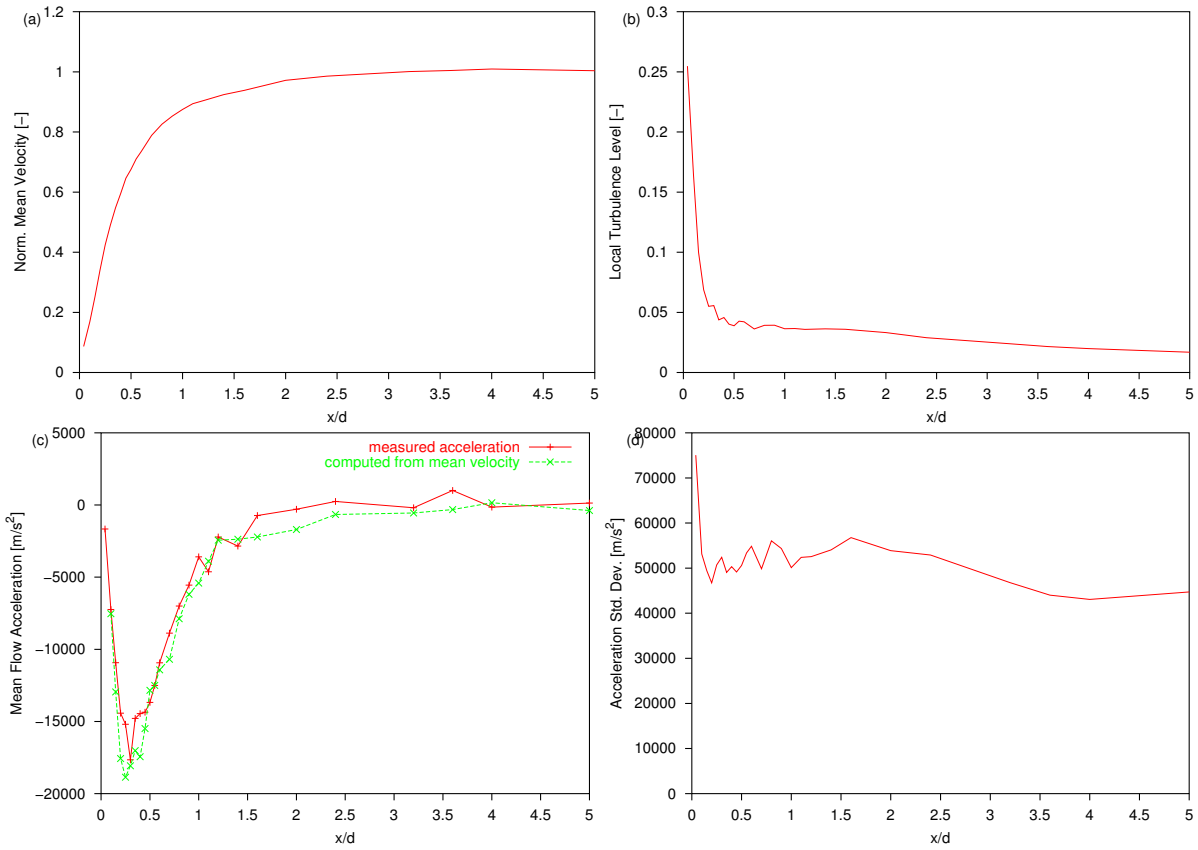

Figure 9: Measurement results from the stagnation flow (a) normalized mean velocity (b) local turbulence level (c) measured and computed flow acceleration (d) standard deviation of measured acceleration

velocity simplifies to

$$\frac{\mathrm{D}}{\mathrm{D}t} = u\frac{\partial u}{\partial x} \tag{50}$$

i.e. the particle acceleration consists only of a convective part. The left-hand side can be measured directly and the right-hand side can be computed from the mean velocity profile. The comparison of these two values is shown in figure 9c, indicating rather good agreement. Noteworthy is the large numerical value of acceleration involved (up to $18\,000\,\mathrm{m/s^2}$).

In figure 9d the standard deviation of the measured acceleration is shown. This quantity exhibits an almost constant value of $50\,000\,\mathrm{m/s^2}$, considerably larger than the mean value itself. To put this value of standard deviation into perspective, the specifications of the optical system were used to express the value in terms of a variance of the acceleration parameters, i.e. $\sigma^2_{\hat{\gamma}}$. A value of $\sigma^2_{\hat{\gamma}} = 5 \times 10^{-12}\,\mathrm{t.u.}^{-4}$ was obtained. Furthermore, several individual signals were analysed to estimate their noise power, resulting in an estimation range of $10^{-5} < \sigma^2_{\mathrm{n}} < 10^{-4}$ [a.u.^{2}]. For these noise levels, an acceleration parameter variance of $\sigma^2_{\hat{\gamma}} < 10^{-13}\,\mathrm{t.u.}^{-4}$ can be expected on the basis of estimator variance alone. The conclusion reached by comparing this value to the measured value ($\sigma^2_{\hat{\gamma}} = 5 \times 10^{-12}\,\mathrm{t.u.}^{-4}$) is that the measured acceleration was physical acceleration variations of the flow and not just statistical fluctuations of the estimator.

One point of discussion is whether the seed particles are able to follow all flow fluctuations at the measured values of acceleration. The equation of particle motion applicable in this case is known as the Basset-Boussinesq-Oseen equation. In this equation, as discussed in detail in [4] the terms accounting for unsteadiness include the virtual mass term and the Basset "history" term. For typical tracer particles of diameter $d_{\mathrm{p}} < 4\,\mu\mathrm{m}$ in air, the latter term becomes insignificant and the particle response exhibits a

low-pass filter behaviour with a time constant equal to

$$\tau = \frac{m_\mathrm{p} + \frac{1}{2} m_\mathrm{f}}{3\mu\pi d_\mathrm{p}} = \frac{d_\mathrm{p}^2(\varrho_\mathrm{p} + \frac{1}{2}\varrho_\mathrm{f})}{18\mu} \tag{51}$$

where μ is the dynamic viscosity of the medium, m_p, d_p and ϱ_p are the mass, the diameter and the density of the particle, m_f and ϱ_f are the virtual mass and the density of the fluid.
For a jump of the flow velocity u_f the particle velocity u_p follows with an exponentially decreasing slip

$$s = \frac{|u_\mathrm{p} - u_\mathrm{f}|}{|u_\mathrm{f}|} \tag{52}$$

Because of the linear character of such a system, a continuously increasing velocity (ramp function) the particle velocity stays behind the flow velocity. The velocity difference increases and becomes asymptotically a constant value. Hence, the particle acceleration increases and ends asymptotically at the value of the flow acceleration. Defining an acceleration slip as

$$s_\mathrm{a} = \frac{|a_\mathrm{p} - a_\mathrm{f}|}{|a_\mathrm{f}|} \tag{53}$$

yields an exponentially decreasing value with the same time constant as given in equation (51).
Therefore, particles which can follow the flow velocity sufficiently also follow the flow acceleration appropriately. Nonetheless, it is still necessary to check whether the time constant of the tracer particles given in equation (51) is small enough to follow the velocity fluctuations over the entire frequency range with significant spectral power densities [2, 21].

5. DISCUSSION AND CONCLUSION

In summary, of the three investigated estimators for the acceleration, the iterative parametric estimator consistently yields the lowest bias and variance, followed in general by the direct parametric and the non-parametric estimation. This directly corresponds to the required computational effort. For a practical application a useful compromise must be found between the required accuracy of the signal parameters and the available data rate. To extend present laser Doppler systems for measurement of acceleration, the non-parametric method is attractive because of its simplicity and robustness and because this method exhibits a lower sensitivity to envelope irregularities than the other estimators. The measured signal must be equalized using for example a discrete Hilbert transform, which can be realized with an FFT routine. Two Gaussian window functions extending over 2/3 of the signal duration and shifted by 1/3 yield two fractional signals, which can be analysed separately using standard frequency estimators known from laser Doppler signal processing (e.g. spectral interpolation). These two frequency estimates directly correspond to the midpoint frequencies of the fractional signals, which can be easily converted to the midpoint frequency of the entire burst and the acceleration. Furthermore, by choosing the width of the Gaussian window function, a balance between the bias and the variance of the estimation can be adjusted. Good results has been obtained with $\xi = 40$ (equation (38)).
This paper has focused on appropriate estimators for acceleration and their performance in terms of expectation and variance. However, in an actual measurement system, also possible systematic errors must be considered, the most important being the fringe uniformity. Depending on the expected trajectories of the particles, both the longitudinal and transverse changes of fringe spacing must be considered. As mentioned in section 4, the Rayleigh length, given by $l_R = \pi r_\omega^2/\lambda$ is the main influencing parameter of fringe non-uniformity for a system in which the waists of the two beams are well-aligned with each other. Here r_ω is the beam waist radius and λ is the wavelength. Miles [17] provides expressions for fringe spacing as a function of l_R and position within the measurement volume. Fringe non-uniformity increases sharply for highly focussed beams or for small intersection angles. In many systems therefore, this systematic error may already exceed the estimator bias and the choice of estimator is no longer critical. In such cases, a non-parametric estimator with a Hanning window function may already be adequate, since it exhibits a bias of the midpoint frequency of less than 0.2 % and for the acceleration parameter less than 6 %.

Extending the signal processing from only frequency estimation to also acceleration estimation adds one more degree of freedom. To achieve the same performance (estimator variance), the signal quality must therefore be higher, or for the same signal quality, the estimator variance will increase. For the non-parametric estimator with a Gaussian window ($\xi = 40$) a variance ratio of 1.2 of the frequency estimation has been found. That means that it is possible to estimate the acceleration from a given Doppler burst with an increased variance of the frequency estimate of 20 %. Note that a frequency estimation without an acceleration estimation in the presence of acceleration leads to a false interpretation, because a constant frequency is assumed. The smaller estimator variance does not necessary imply higher accuracy.
Alternatively, the above statement can be interpreted in terms of SNR. To achieve a given frequency estimator variance, an increase in SNR of 0.8 dB is necessary if also acceleration is being estimated.
The present experiments indicate that the numerical values of acceleration encountered in turbulent flows are high. The verification results in figure 9c indicate that these results are reliable. Also other investigations confirm that such high values are plausible [14, 24]. Furthermore, the estimations performed for the present laser Doppler system show that the estimation variance is smaller than the measured acceleration variance by a factor of approximately 10^{-2}. Thus, it can be concluded that the methods introduced here are very appropriate for the measurement of acceleration in turbulent flows.
Finally, the application of these methods to measure acoustic waves can be examined. This will depend very much on the circumstances. If the acoustic wave is present in stagnant surroundings and for system and noise specifications similar to those used in the present experiments, values of acceleration down to about $1\,000\,\mathrm{m/s^2}$ could be resolved. In the range of audiable frequencies, this corresponds to rather high values of SPL. For ultrasonic applications on the other hand, e.g. $f = 20$–$50\,\mathrm{kHz}$, acoustic measurements are quite feasible.
The situation is not so promising if the acoustic waves are embedded in a turbulent flowfield. In this case the acceleration due to turbulence can easily exceed $10^5\,\mathrm{m/s^2}$, which would generally dominate all acoustic accelerations, except possibly for those originating from strong ultrasonic fields.

The authors gratefully acknowledge the help of J Helbig (DLR) in performing the experiments and developing the signal processing programs.

REFERENCES

[1] J S Bendat and A G Piersol. *Random data, analysis and measurement procedures.* John Wiley and Sons, New York, 1986.

[2] L H Benedict, H Nobach, and C Tropea. Estimation of turbulent velocity spectra from laser Doppler data. *Meas. Sci. Technol.*, 11(8):1089–1104, 2000.

[3] K T Christensen and R J Adrian. Measurement of instantaneous acceleration fields using particle-image velocimetry. In *PIV01 Conference*, Göttingen, Germany, 2001. paper 1080.

[4] C Crowe, M Sommerfeld, and Y Tsuji. *Multiphase Flows with Droplets and Particles.* CRC Press LLC, Boca Raton, 1998.

[5] J Domnick, H Ertl, and C Tropea. Processing of phase/Doppler signals using the cross spectral density function. In *Proc. 4th Int. Symp. on Appl. of Laser Techn. to Fluid Mechanics*, Lisbon, Portugal, 1988. paper 3.8.

[6] E Gledzer. On the Taylor hypothesis correlations for measured energy spectra of turbulence. *Physica D*, 104:163–183, 1997.

[7] R J Hill and S T Thoroddsen. Experimental evaluation of acceleration correlations for locally isotropic turbulence. *Phys Rev E*, 55:1600–1606, 1997.

[8] K Hishida, K Kobashi, and M Maeda. Improvement of LDA/PDA using a digital signal processor (DSP). In *Proc. 3rd Int. Conf. on Laser Anemometry*, Swansea, UK, 1989. paper S2.

[9] M Kendal and A Stuart. *The Advanced Theory of Statistics*, volume 2. Charles Griffin, London, 1963.

[10] A N Kolmogorov. Dissipation of energy in the locally isotropic turbulence. *Dokl. Akad. Nauk SSSR*, 31:538–540, 1941.

[11] A N Kolmogorov. The local structure of turbulence in incompressible viscous fluid for very large Reynolds numbers. *Dokl. Akad. Nauk SSSR*, 30:301–305, 1941.

[12] B Lehmann, A Helbig, and C Hassa. LDA method to measure the acceleration of particles and the curvature radii of particle trajectories. In *Proc. 5th Int. Symp. on Appl. of Laser Techn. to Fluid Mechanics*, Lisbon, Portugal, 1990. paper 22.3.

[13] B Lehmann and A Helbig. Laser-Doppler-Messung lokaler Beschleunigungen in turbulenter Strömung. In *Proc. 7. Fachtagung Lasermethoden in der Strömungsmeßtechnik*. Shaker-Verlag Aachen, 1999. Beitrag 4.

[14] B Lehmann and J Helbig. Local acquisition of mean and turbulent fluid acceleration in highly turbulent flow by the means of laser-Doppler velocimetry. In *Proc. 10th Int. Symp. on Appl. of Laser Techn. to Fluid Mechanics*, Lisbon, Portugal, 2000.

[15] C C Lin. On Taylor's hypothesis in wind tunnel turbulence. *Q. Appl. Math.*, 10:295, 1953.

[16] D Matovic and C Tropea. Spectral peak interpolation with application to LDA signal processing. *Meas. Sci. Technol.*, 2:1100–1106, 1991.

[17] P C Miles. Geometry of the fringe field formed in the intersection of two Gaussian beams. *Appl Optics*, 35:5887–5895, 1996.

[18] A S Monin and A M Yaglom. *Statistical Fluid Mechanics Vol II*. MIT Press, Cambridge, Massachusetts, USA, 1975. Sec. 18.

[19] H Nobach, C Schneider, A Dreizler, J Janicka, and C Tropea. Laser-Doppler-Messungen von Teilchenbeschleunigungen und der Dissipationsrate in einem runden Freistrahl. In *Proc. 10. Fachtagung Lasermethoden in der Strömungsmeßtechnik*, 2002.

[20] H Nobach and H R E van Maanen. LDA and PDA signal analysis using wavelets. *Experiments in Fluids*, 30:613–625, 2001.

[21] H Nobach. Local time estimation for the slotted correlation function of randomly sampled LDA data. *Exp. in Fluids*, 32:337–345, 2002.

[22] A Papoulis. *Probability, Random Variables and Stochastic Processes*. McGraw-Hill, New York, 1988.

[23] M Pinsky, A Khain, and A Tsinober. Accelerations in isotropic and homogeneous turbulence and Taylor's hypothesis. *Phys Fluids*, 12:3195–3204, 2000.

[24] A La Porta, G A Voth, A M Crawford, J Alexander, and E Bodenschatz. Fluid particle accelerations in fully developed turbulence. *Nature*, 409:1017–1019, 2001.

[25] V Prakash and P K Yeung. Similarity scaling of acceleration and pressure statistics in numerical simulations of isotropic turbulence. *Phys of Fluids*, 11:1208–1220, 1999.

[26] H Tennekes and J L Lumley. *A first course in turbulence*. MIT Press, Cambridge, Massachusetts, USA, 1972.

[27] G A Voth, K Satyanarayan, and E Bodenschatz. Lagrangian acceleration measurements at large Reynolds numbers. *Phys Fluids*, 10:2268–2280, 1998.

[28] P K Yeung and S B Pope. Lagrangian statistics from direct numerical simulations of isotropic turbulence. *J. Fluid Mech.*, 207:531, 1982.